

# Quantum Multibaker Maps I: Extreme Quantum Regime

Daniel K. Wójcik\*

*Institute for Physical Science and Technology,  
University of Maryland,  
College Park, MD, 20742, USA and  
Centrum Fizyki Teoretycznej Polskiej Akademii Nauk,  
Al. Lotników 32/46, 02-668 Warszawa, Poland;*

J. R. Dorfman

*Institute for Physical Science and Technology,  
and Department of Physics  
University of Maryland, College Park, MD, 20742, USA  
(Dated: January 30, 2020)*

We introduce a family of models for quantum mechanical, one-dimensional random walks, called quantum multibaker maps (QMB). These are Weyl quantizations of the classical multibaker models previously considered by Gaspard, Tasaki and others. Depending on the properties of the phases parametrizing the quantization, we consider two classes of the QMB maps: regular and random. Regular QMB maps are characterized by phases which are the same in every unit cell of the multibaker chain. They have spatially extended eigenstates and exhibit ballistic transport. Random QMB maps have phases that vary randomly from unit cell to unit cell. They have localized eigenstates and exhibit subdiffusive transport. In the regular case and for large  $\hbar$ , analytic solutions can be obtained for the time dependent quantum states for periodic chains and for open chains with absorbing boundary conditions. Steady state solutions and the properties of the relaxation to a steady state for a regular QMB chain in contact with “particle” reservoirs can also be described analytically. The analytical results are consistent with, and confirmed by, results obtained from numerical methods. We report here results for the deep quantum regime (large  $\hbar$ ) of the regular QMB, as well as some results for the random QMB. We leave the moderate and small  $\hbar$  results as well as further consideration of the other versions of the QMB for further publications.

PACS numbers: 05.60.Gg, 05.60.-k, 03.65.-w

## I. INTRODUCTION

The quantum mechanics of classically chaotic systems, often called quantum chaos, is by now a highly developed subject with an enormous literature, including monographs by Gutzwiller [1], Stöckmann [2], and Haake [3], among others. The subject has been greatly advanced, as is usual, by detailed analyses of simple model systems such as kicked rotors, quantum flows on surfaces of constant negative curvature, Harper models, and so on. Some of the central problems that have been studied using these models include those of: (1) finding explanations for the efficacy of random matrix theories, (2) understanding the differences between quantum and classical transport, especially when Anderson localization plays a role in the quantum system, (3) studying the properties of quantum systems in the semi-classical limit, and (4) determining the role of decoherence in producing classically chaotic behavior of a quantum system as Planck’s constant tends to zero.

The present paper treats the quantum versions of sim-

ple model systems, multibaker maps, that have been used to study transport phenomena in classically chaotic systems. A multibaker map consists of a chain of two-dimensional baker maps which are interconnected by means of a simple change in the baker dynamics. In the usual baker map on a unit square or torus, two vertical strips are stretched (by a factor of two) in the horizontal direction, contracted (by a factor of two) in the vertical direction, and the resulting horizontal strips are placed one above the other, in order to reconstruct the unit square. In the multibaker chain, each of the two horizontal rectangles are sent to adjacent cells, one to the right and the other to the left (Fig. 1). Modified multibaker chains have also been studied where there may be more strips and/or a more complicated dynamics including both area preserving and area non-preserving dynamics. These classical models provide simple, deterministic models of one dimensional random-walk processes with both diffusive transport and chaotic dynamics. They have been used to study connections between transport properties such as transport coefficients, and irreversible entropy production, and the chaotic properties of the models [4, 5, 6, 7, 8, 9, 10, 11, 12, 13, 14, 15, 16, 17, 18].

Quantum versions of baker maps are well known and studied in some detail for a range of values of Planck’s constant. Here we add a mechanism for transport of

---

\*Electronic address: danek@ipst.umd.edu; URL: <http://www.cft.edu.pl/~danek>

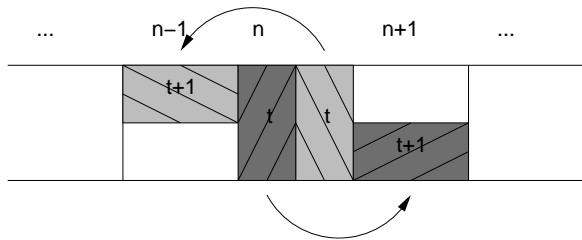


FIG. 1: Classical multibaker model.

probability amplitudes along a one dimensional chain of quantum baker maps. This quantum version of the multibaker map (QMB) provides one realization of a quantum random walk process. In this paper we will concentrate on the “most quantum” version of the QMB, obtained by using the largest possible value of Planck’s constant  $\hbar = 1/2$ , in the Weyl quantization of the ordinary baker map [19, 20]. Our goal here will be to explore the transport properties of the QMB for this value of  $\hbar$ , and for two different versions of the model, obtained by taking advantage of some phase-related arbitrariness in the quantization of the map. Later papers will explore further properties of QMB’s including the semi-classical case, not considered here [21, 22].

Area-preserving maps on torus admit a two-parameter family of Weyl quantizations [20, 23, 24], where the two parameters can be chosen to be phases. One can think of the two phases as offsets of lattice points that define the spatial and momentum coordinates of the map. If we choose the same phases in each unit cell of the chain, we have a “regular” QMB. If we choose random phases from cell to cell, we obtain a “random” QMB. The different versions have quite different properties, as one might expect. The regular QMB has many features in common with periodic quantum crystals, including extended eigenstates, and ballistic transport, while the random case exhibits the usual phenomena associated with localization. Nevertheless, there are some interesting surprises, as we shall see in further sections, associated with transport in open systems.

There are a number of formulations of quantum random walks already in the literature. We mention, in particular, work of Aharonov *et al.* [25], work of Godoy *et al.* [26, 27], and work of Barra and Gaspard [28]. The papers of Godoy and co-authors as well as that of Barra and Gaspard have interesting parallels with ours. These authors consider the motion of a quantum particle along a one-dimensional, periodic chain of scattering sites. The scattering sites are characterized by transmission and reflection amplitudes, which for a periodic system, are taken to be the same for each site. Godoy and co-workers consider the wave functions for their systems at discrete positions and discrete times, and propose a set of equations similar to the ones considered here. These equations are then solved using stationary phase approximations, and the connections with Landauer’s formula are discussed, for various parameters and particle statistics.

Barra and Gaspard also consider a model similar to ours, and they analyze the scattering resonances for a finite, open system. By applying transfer and  $S$  matrices, they obtain expressions for the widths of resonances and the Wigner time delay, as functions of the system size. Their equations are in fact quite similar to ours, and a number of results differ in the two cases only because of the differences in the details of the model studied. Their model has two channels per cell (particles moving to the left or right) but the particles can have a wide range of energies, and in some instances the high-energy limit is considered. The similarities with the work of Godoy *et al.* occur because the version of the quantum multibaker model considered in the present paper is the simplest possible, while more complicated versions, to be considered in further papers have no direct counterparts in their work.

Despite the similarities between our work and that of other authors, the focus of the work mentioned above generally differs from ours. We are particularly interested in comparing and contrasting quantum and classical multibaker maps, and in generalizing the QMB in a number of directions. These include an examination of the behavior of the QMB for smaller values of  $\hbar$  including the semi-classical limit, and looking for traces, if any, of the chaotic classical behavior in the quantum version. The present paper is designed to identify important quantum phenomena that differ from those of the classical multibaker at large  $\hbar$ , but which are expected to approach the classical results as the Planck’s constant,  $\hbar = 1/N$ , tends to zero.

The plan of the paper is as follows: In Section II we will define the classical version of the model and study the evolution of piecewise constant probability densities. In Section III we quantize the multibaker map using Weyl quantization. There we will define the regular and random QMB’s and obtain expressions for the time dependent propagator appearing in the discrete time version of Schrödinger’s equation. In Section IV we describe the behavior of the regular QMB for  $\hbar = 1/2$ . We find the eigenstates for both closed and open systems, as well as the steady state solutions for systems with particle reservoirs at their boundaries. We then consider the transport properties of particles in these chains. Of particular interest in this connection is our finding that for open chains of regular multibakers, and with absorbing boundary conditions, the escape of particles from the chain is *subdiffusive* despite the ballistic transport of particles from the interior of the chain to its boundaries. We then turn to a brief discussion of the properties of random multibakers and show that the assumption of random phases leads to localized wavefunctions with very different properties from the regular case. Our results are summarized and discussed in Section VI.

## II. THE CLASSICAL MULTIBAKER MAP

The classical multibaker map provides a reversible, deterministic realization of a one-dimensional random walk. It is the simplest area-preserving, deterministic model for diffusion of a particle on a one dimensional lattice, whereby the particle makes steps either to the right or left at equally spaced time intervals. The multibaker map can be adjusted for any set of step probabilities,  $p, q = 1 - p, 0 \leq p, q \leq 1$ , where  $p$  is the probability of making a step to the right. The classical multibaker map is based upon the usual baker's map,  $\mathbf{B}$  on the unit square,  $(0 \leq x, y < 1)$ , defined by

$$\mathbf{B}(x, y) = \begin{cases} (x/p, py), & \text{for } 0 \leq x \leq p, \\ ((x-p)/q, p+qy), & \text{for } p < x < 1. \end{cases} \quad (1)$$

The multibaker map is constructed by taking a linear chain of  $L$  adjacent unit squares, labeled by the index  $n, n = 0, \dots, L-1$ , such that any point on the chain is labeled by the three quantities,  $n, x, y$  with  $0 \leq x, y < 1$ . Then the action of the map,  $\mathbf{M}$  on any point is obtained by combining a baker's map with translation of each rectangle to the right or left, as given by

$$\begin{aligned} \mathbf{M}(n, x, y) &= (n+1, x/p, py), \text{ for } 0 \leq x \leq p, \\ &= (n-1, (x-p)/q, p+qy), \text{ for } p < x < 1. \end{aligned} \quad (2)$$

This arrangement has the property that there is a probability  $p$  of choosing a point which moves one square to the right, and probability  $q$  of choosing a point which moves one square to the left. To complete the specification of the map, one must append boundary conditions to the transformation given by Eq. (2). Such conditions may include periodic, or absorbing boundary conditions, or one might specify that the ends of the chain are connected to reservoirs which maintain a constant density of points at the boundaries. As a chaotic system, the multibaker map is a measure preserving map with positive and negative Lyapunov exponents, given by  $\lambda_{\pm} = \pm[p \ln(1/p) + q \ln(1/q)]$ . This map has been used to study the properties of deterministic diffusion in a chaotic system, studies of the connection between diffusion coefficients and Lyapunov exponents for an open chain, a study of entropy production in the relaxation to a uniform equilibrium state, and has been extended to provide simple models for viscous and heat flows as well [4, 5, 6, 7, 8, 9, 10, 11, 12, 13, 14, 15, 16, 17, 18].

The classical version of the quantum multibaker considered here was discussed in [8]. We consider here a simple form of this classical model constructed to be a classical version of the  $\hbar = 1/2$  quantum system. We will study the evolution of probability densities integrated along the stable direction ( $y$ ) and piecewise constant on two halves of every multibaker cell (along the unstable direction). This space of densities is  $2L$  dimensional. Therefore, the evolution operator for this class of probability densities has the same dimension as the quantum multibaker propagator considered in Section III.

### A. Closed, periodic case

We consider the classical evolution of phase space densities under the dynamics given by Eq. (2) with  $p = 1/2$ . Since the quantum version will describe probability amplitudes in either space or momentum, the classical counterparts are obtained by projecting the classical densities along the  $x$  or  $y$ -axes, respectively. We restrict our attention to probability densities projected onto the unstable  $x$ -direction and we take them to be constant on intervals  $0 \leq x < 1/2$ ,  $1/2 \leq x < 1$ ,  $n = \text{const}$ , to mimic the  $\hbar = 1/2$  quantum case. Then the projected distribution is

$$\begin{aligned} \varrho(n, x, t) &:= \int_0^1 \varrho(n, x, y, t) dy \\ &= \begin{cases} \varrho_L(n, t), & \text{for } 0 \leq x < 1/2, \\ \varrho_R(n, t), & \text{for } 1/2 \leq x < 1. \end{cases} \end{aligned} \quad (3)$$

and it satisfies a Frobenius-Perron equation given by

$$\varrho_{L,R}(n, t+1) = \frac{1}{2}[\varrho_L(n-1, t) + \varrho_R(n+1, t)], \quad (4)$$

with periodic boundary conditions  $\varrho_{L,R}(n+L, t) = \varrho_{L,R}(n, t)$ . Since this equation is linear we may suppose that  $\varrho_{L,R}(n, t)$  represent the deviations from a uniform equilibrium state, and may take both positive and negative values. An eigenstate of the right hand side of Eq. (4) satisfies

$$\lambda \varrho_L(n) = \lambda \varrho_R(n) = \frac{1}{2}[\varrho_L(n-1) + \varrho_R(n+1)]. \quad (5)$$

It follows that either  $\lambda = 0$  or  $\varrho_L(n) = \varrho_R(n)$ . Clearly, the  $L$  vectors of the form

$$\begin{aligned} \varrho_L(k-1) &= -\varrho_R(k+1) \neq 0, \\ \varrho_L(n \neq k-1) &= \varrho_R(n \neq k+1) = 0, \end{aligned}$$

belong to the kernel,  $\lambda = 0$ , of the classical discrete multibaker. For the case where  $\lambda \neq 0$  we look for solutions of the form  $\varrho_{L,R}(n) = A e^{in\vartheta}$  and Eq. (4) leads to  $\lambda = \cos \vartheta$ . The general solution is, then,  $\varrho_{L,R}(n) = A_1 \cos(\vartheta n) + A_2 \sin(\vartheta n)$ , where periodic boundary conditions lead to  $\vartheta = 2k\pi/L$ , and the normalized eigenstates can readily be determined. For odd  $L = 2M+1$  we have the  $L$  solutions

1.  $M$  solutions of the form  $\varrho_{L,R}(n) = A \cos \frac{2k\pi n}{L}$ ,  $\lambda = \cos \frac{2k\pi}{L}$ ;  $k = 1, \dots, \frac{L-1}{2}$ ;
2.  $M$  solutions of the form  $\varrho_{L,R}(n) = A \sin \frac{2k\pi n}{L}$ ,  $\lambda = \cos \frac{2k\pi}{L}$ ;  $k = 1, \dots, \frac{L-1}{2}$ ;
3. 1 solution  $\varrho_{L,R}(n) = A$ ,  $\lambda = 1$ ;  $k = 0$ .

For even  $L = 2M$  we have the  $L$  solutions

1.  $M-1$  solutions of the form  $\varrho_{L,R}(n) = A \cos \frac{2k\pi n}{L}$ ,  $\lambda = \cos \frac{2k\pi}{L}$ ;  $k = 1, \dots, \frac{L}{2} - 1$ ;

2.  $M - 1$  solutions of the form  $\varrho_{L,R}(n) = A \sin \frac{2k\pi n}{L}$ ,  $\lambda = \cos \frac{2k\pi}{L}$ ;  $k = 1, \dots, \frac{L}{2} - 1$ ;
3. 1 solution  $\varrho_{L,R}(n) = A$ ,  $\lambda = 1$ ;  $k = 0$ , and,
4. 1 solution  $\varrho_{L,R}(n) = (-1)^n A$ ,  $\lambda = -1$ ;  $k = M = L/2$ .

We see that in the odd case there is an approach to equilibrium: all the eigenvalues have absolute value strictly less than 1, apart from the one corresponding to the uniform distribution. The even case is sensitive to the “even-odd” oscillations of the location of a point along

the chain. These oscillations can be removed by combining two successive steps.

### B. Open case (absorbing boundary conditions)

For the open chain with absorbing boundary conditions, the dynamics inside is the same as in the closed case and is given by Eq. (4), therefore the general solution is also given by  $\varrho_{L,R}(n) = A_1 \cos(\vartheta n) + A_2 \sin(\vartheta n)$ . Absorbing boundary conditions  $\varrho_{R,L}(-1) = \varrho_{R,L}(L) = 0$  lead to

$$\lambda A_1 = \frac{1}{2}[A_1 \cos \vartheta + A_2 \sin \vartheta], \quad (6)$$

$$\lambda[A_1 \cos(L-1)\vartheta + A_2 \sin(L-1)\vartheta] = \frac{1}{2}[A_1 \cos(L-2)\vartheta + A_2 \sin(L-2)\vartheta], \quad (7)$$

where  $\lambda = \cos \vartheta$ . They have nontrivial solutions if and only if  $\sin(L+1)\vartheta = 0$ , leading to  $\vartheta_k = \frac{k\pi}{L+1}$ , where  $k = -L, \dots, -1, 1, \dots, L$ , and  $\lambda(-\vartheta) = \lambda(\vartheta)$ . Thus finally  $k = 1, \dots, L$ , which gives the  $L$  states of the form

$$\varrho_{L,R}(n) = A \sin \frac{k(n+1)\pi}{L+1}. \quad (8)$$

The remaining  $L$  states are in the kernel:  $L-2$  are of the form given by Eq. (6) with  $n = 1, \dots, L-2$ . Two other states corresponding to  $\lambda = 0$  are  $\varrho_L(L-1) = 1$ ,  $\varrho_L(k \neq L-1) = \varrho_R(k) = 0$ , and  $\varrho_R(0) = 1$ ,  $\varrho_R(k \neq 0) = \varrho_L(k) = 0$ . Thus we easily obtain a spectral decomposition for the simple operator treated here, with absorbing boundary conditions.

The probability of finding the particle in the system decays with the escape rate

$$\gamma := -\lim_{t \rightarrow \infty} \frac{\log P(t)}{t}, \quad (9)$$

where  $P(t) := \sum_n \varrho(n, t)$ , given by the largest eigenvalue

$$\gamma = -\log \left| \cos \frac{\pi}{L+1} \right| \approx \frac{\pi^2}{2L^2}, \quad (10)$$

for large  $L$ .

### C. The open, discrete multibaker with reservoirs

Next we connect particle reservoirs to a finite chain and look for steady state solutions. These are time invariant solutions to Eq. (4), with the boundary conditions

$$\varrho_L(0) = \varrho_R(0) = \frac{1}{2}[\varrho_1 + \varrho_R(1)], \quad (11)$$

$$\varrho_L(L-1) = \varrho_R(L-1) = \frac{1}{2}[\varrho_L(L-1) + \varrho_2], \quad (12)$$

where  $\varrho_1, \varrho_2$  are the incoming densities of the left and right reservoirs, respectively. A solution is found immediately by observing that in the steady state  $\varrho_L(n) = \varrho_R(n) \equiv \varrho(n)$  and that Eq. (4) leads to  $\varrho(n+1) = 2\varrho(n) - \varrho(n-1)$ . A solution satisfying the boundary conditions is therefore

$$\varrho(n) = \frac{\varrho_2 + L\varrho_1}{L+1} + \frac{n(\varrho_2 - \varrho_1)}{L+1}. \quad (13)$$

The linear profile expected from the Fick's law [4, 8, 9] is shown in Figure 2.

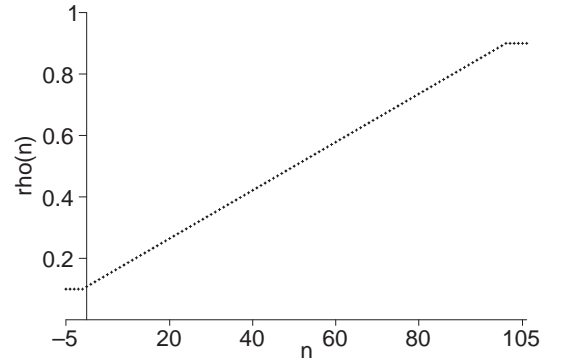


FIG. 2: Linear profile of the classical discrete multibaker map of length  $L = 101$  with reservoirs ( $\varrho_1 = 0.1, \varrho_2 = 0.9$ ). The horizontal axis range is  $[-5, 105]$ .

## III. QUANTUM MULTIBAKER MAP: THE GENERAL MODEL

In order to quantize the multibaker map, we start with the quantum baker map, as described by Balazs, Voros

[19], and Saraceno [20], and then produce a quantum multibaker map by forming a chain of unit squares, applying the quantum baker map to each square, but transferring the new quantum states to the adjacent squares according to the procedure used in the classical case.

The method for constructing a quantum version of the regular baker map is as follows. We consider the  $x$ -direction to be the “spatial” direction of the system, and the  $y$ -direction to be the “momentum” direction. Then the number of quantum states  $N$  in the unit square should satisfy  $N = PQ/2\pi\hbar$ , where  $Q = 1$  is the spatial extent of the unit square, and  $P = 1$  is the range of momenta. This leads to the simple formula,  $\hbar = 1/(2\pi N)$ , where  $N$  is an integer. We usually, but not always, take  $N$  to be an even integer, so that one half of the quantum states can be associated with each half of the unit square. One then constructs a set of  $N$  “position” states for a unit square, with position eigenvalues  $q_j = 2\pi\hbar(j + \varphi_q) = (j + \varphi_q)/N$ ,  $j = 0, \dots, N-1$  and a set of  $N$  “momentum” states with momentum eigenvalue  $p_k = 2\pi\hbar(k + \varphi_p) = (k + \varphi_p)/N$ ,  $k = 0, \dots, N-1$ . We require that  $0 \leq \varphi_{q,p} < 1$ . The position and momentum states are related to each other by means of a simple Fourier representation, with  $N$  terms, given by

$$(G_N)_{kj} \equiv \langle p_k | q_j \rangle = \frac{1}{\sqrt{N}} e^{-2\pi i(k+\varphi_p)(j+\varphi_q)/N}. \quad (14)$$

We include subscripts on  $p, q$  in the notation for the Dirac matrix element to identify the integers which are attached to the  $p$  and  $q$  representations. The phases,  $\varphi_q, \varphi_p$  are as yet unspecified. In the literature on the quantum baker map, these phases are often taken to be 0 (the simplest [19]) or 1/2 (most symmetric map [20]). Here we will take advantage of the possibility to choose these phases so as to represent different situations that may have some relevance to physical phenomena.

The time dependence of the quantum baker map is determined by constructing a propagator for the change in the quantum states over one time step. This propagator consists of two parts: First one transforms the “left” part of the Hilbert space (in the position representation) into “bottom” subspace (in momentum representation) and the “right (position) part” into the “top (momentum) part”. Then one uses the Fourier relation between position and momentum states, Eq. (14), to change the basis from momentum back to position representation. The first transformation consists of two Fourier transforms over  $N/2$ -dimensional space, the other is the inverse Fourier transform over the whole  $N$ -dimensional

space.

$$\mathbf{B}_q = [G_N^{-1}] \cdot \begin{bmatrix} G_{N/2} & 0 \\ 0 & G_{N/2} \end{bmatrix}. \quad (15)$$

The action of  $\mathbf{B}_q$  on a position-space wave function is understood as follows. We represent the position-space function as a column vector with  $N$  elements, the top  $N/2$  elements referring to the quantum states with numbers  $j = 0, 1, \dots, (N/2) - 1$ , which we denote as the “left” states. The bottom  $N/2$  elements having quantum numbers  $j = N/2, N/2 + 1, \dots, N - 1$ , are called the “right” states. The block diagonal matrix, with blocks  $G_{N/2}$  appearing on the right hand side of Eq. (15) transfers the left and right spatial states to the “bottom” and “top” momentum states, respectively, according to

$$\begin{bmatrix} \tilde{\Psi}_b(t+1) \\ \tilde{\Psi}_t(t+1) \end{bmatrix} = \begin{bmatrix} G_{N/2}(\varphi_q, \varphi_p) & 0 \\ 0 & G_{N/2}(\varphi_q, \varphi_p) \end{bmatrix} \cdot \begin{bmatrix} \Psi_l(t) \\ \Psi_r(t) \end{bmatrix}. \quad (16)$$

This operation defines the quantum baker map. However, we are left with a quantum state in the momentum representation. We now change the momentum state representation into a spatial state by means of the matrix  $G_N^{-1}$ , as in Eq. (14).

Finally we can construct a *quantum multibaker* map (QMB) by considering a chain of unit squares, each taken to be an individual quantum system, but which exchange quantum states according to the rules of the quantum baker with an interlacing process formed in analogy with the classical multibaker map Eq. (2). That is, the position space functions at site  $n$  are transformed to momentum space functions at sites  $n \pm 1$ , according to the rule

$$\begin{bmatrix} \tilde{\Psi}_b(n+1, t+1) \\ \tilde{\Psi}_t(n-1, t+1) \end{bmatrix} = \begin{bmatrix} G_{N/2}(n) & 0 \\ 0 & G_{N/2}(n) \end{bmatrix} \cdot \begin{bmatrix} \Psi_l(n, t) \\ \Psi_r(n, t) \end{bmatrix}. \quad (17)$$

Here we can allow for the phases  $\varphi_{q,p}(n)$  to vary from one cell, denoted by  $n$ , to the next, and we incorporate them in the transformation operators  $G_N(n) \equiv G_N(\varphi_q(n), \varphi_p(n))$  at that site. After this transformation is carried out, we change from the momentum to the position representation at each site according to the same rule as in an ordinary quantum baker map, that is

$$\begin{bmatrix} \Psi_l(n, t+1) \\ \Psi_r(n, t+1) \end{bmatrix} = G_N^{-1}(n) \cdot \begin{bmatrix} \tilde{\Psi}_b(n, t+1) \\ \tilde{\Psi}_t(n, t+1) \end{bmatrix}. \quad (18)$$

---

Thus in the position representation the quantum multibaker map is given by

$$\begin{bmatrix} \Psi_l(n, t+1) \\ \Psi_r(n, t+1) \end{bmatrix} = G_N^{-1}(n) \cdot \begin{bmatrix} G_{N/2}(n-1) & 0 \\ 0 & G_{N/2}(n+1) \end{bmatrix} \cdot \begin{bmatrix} \Psi_l(n-1, t) \\ \Psi_r(n+1, t) \end{bmatrix}. \quad (19)$$

Explicitly, we have

$$\Psi_l(n, t+1) = [G_N^{-1}(n)]_{l,b} \cdot G_{N/2}(n-1) \cdot \Psi_l(n-1, t) + [G_N^{-1}(n)]_{l,t} \cdot G_{N/2}(n+1) \cdot \Psi_r(n+1, t), \quad (20)$$

$$\Psi_r(n, t+1) = [G_N^{-1}(n)]_{r,b} \cdot G_{N/2}(n-1) \cdot \Psi_l(n-1, t) + [G_N^{-1}(n)]_{r,t} \cdot G_{N/2}(n+1) \cdot \Psi_r(n+1, t). \quad (21)$$

Here, in an obvious notation, the matrices  $[G_N^{-1}]_{\alpha,\beta}$  are  $N/2 \times N/2$  block sub-matrices that comprise  $G_N^{-1}$ . The general case can be treated numerically, of course, once the phases are specified. It is of interest to consider the special case  $N = 2$ , since much of the work can be done using simple analytical methods, and since this case corresponds to the largest possible value for Planck's constant, namely,  $\hbar = 1/2$ . This is the case we study here.

The local dynamics are characterized by the two phases,  $\varphi_q, \varphi_p$ , which parameterize the Weyl quantizations of the baker map. If we take the same pair of phases at each site we obtain the *regular* model. If we choose them randomly from some distribution at each of the sites, we get the *random* model. In this paper, when we treat the random model we will assume that the phases are chosen according to a uniform distribution on the unit circle [35].

A complete specification of the model is obtained by adding the boundary conditions to the above equations. In this work we restrict our attention to the closed case (with periodic boundary conditions), and open cases (with either absorbing boundary conditions or with “particle” reservoirs at the ends of the chain).

#### IV. REGULAR QUANTUM MULTIBAKER

The regular quantum multibaker is characterized by a set of phases  $\varphi_q, \varphi_p$  that are independent of the site index, that is, they are the same for each of the transformation matrices generating the map, as described in Eq. (19). This makes transport in the regular multibaker chain similar in many respects to transport in a one-dimensional periodic solid. Here we solve this model for time dependent and stationary quantum states with appropriate boundary conditions: the closed, periodic chain; the open chain with absorbing boundary conditions; and the open chain attached to leads at each end, producing a stationary, non-equilibrium state. We begin with the periodic chain.

##### A. Closed, periodic case

We consider the periodic, regular multibaker chain, with  $L$  sites and  $N = 2$ . The equation connecting the quantum states at time  $t+1$  to those at time  $t$  is

$$\begin{aligned} \Psi_l(n, t+1) &= f_0(g_{00}\Psi_l(n-1, t) + g_{01}\Psi_r(n+1, t)), \\ \Psi_r(n, t+1) &= f_0(g_{10}\Psi_l(n-1, t) + g_{11}\Psi_r(n+1, t)). \end{aligned}$$

with  $(0 \leq \varphi_q, \varphi_p < 1)$ , and  $f_0, g_{kl}$  given by

$$\begin{aligned} f_0 &= (G_1(\varphi_q, \varphi_p))_{00} = e^{-i2\pi\varphi_q\varphi_p}, \\ g_{kl} &= (G_2^{-1}(\varphi_q, \varphi_p))_{kl} = \frac{1}{\sqrt{2}}e^{i\pi(k+\varphi_q)(l+\varphi_p)}. \end{aligned} \quad (22)$$

Since the system is periodic, Bloch's theorem guarantees the existence of eigenstates of the form

$$\Psi_{r,l}(n) = A_{r,l}\chi^n = A_{r,l}e^{in\vartheta}. \quad (23)$$

Periodic boundary conditions,  $\Psi(L) = \Psi(0)$ , imply that  $\vartheta = 2k\pi/L$ ,  $k = 0, \dots, L-1$ . Clearly,  $\lambda$  is an eigenvalue of the quantum multibaker propagator if and only if

$$\begin{vmatrix} g_{00}f_0e^{-i\vartheta} - \lambda & g_{01}f_0e^{i\vartheta} \\ g_{10}f_0e^{-i\vartheta} & g_{11}f_0e^{i\vartheta} - \lambda \end{vmatrix} = 0. \quad (24)$$

Using the notation

$$\begin{aligned} \alpha &= (1 + \varphi_q + \varphi_p)\pi/2, \\ \beta &= (1 + \varphi_q + \varphi_p - 2\varphi_q\varphi_p)\pi/2 = \alpha - \pi\varphi_q\varphi_p, \end{aligned} \quad (25)$$

we find that

$$\lambda = \frac{e^{i\beta}}{\sqrt{2}}[\cos(\vartheta + \alpha) \pm i\sqrt{1 + \sin^2(\vartheta + \alpha)}]. \quad (26)$$

Note that (24) can also be written as

$$\begin{aligned} \lambda/e^{i\beta} + e^{i\beta}/\lambda &= \frac{1}{\sqrt{2}}[e^{i(\alpha+\vartheta)} + e^{-i(\alpha+\vartheta)}], \\ v + \frac{1}{v} &= \frac{1}{\sqrt{2}}\left[u + \frac{1}{u}\right], \end{aligned} \quad (27)$$

where  $u = \chi e^{i\alpha}$ ,  $v = \lambda/e^{i\beta}$ . Since  $\vartheta$  is real it follows that  $|\lambda|^2 = 1$ , so  $\lambda = e^{i\gamma}$  and  $\gamma - \beta \in [\pi/4, 3\pi/4] \cup [5\pi/4, 7\pi/4]$ . Therefore the “quasi-energies”,  $\gamma$ , lie in two bands of length  $\pi/2$  symmetric with respect to the center of the unit circle. The exact location depends upon the phases  $\varphi_q, \varphi_p$ . Making use of the boundary conditions we obtain the eigenvalues of the closed multibaker map

$$\lambda_{\pm,k} = \frac{e^{i\beta}}{\sqrt{2}}\left[\cos(\alpha + 2k\pi/L) \pm i\sqrt{1 + \sin^2(\alpha + 2k\pi/L)}\right], \quad (28)$$

with  $\alpha$  and  $\beta$  given by Eq. (25). The corresponding eigenstates are given by Eq. (23) with the constants connected by  $A_r = A_l[\sin(\alpha + 2k\pi/L) \mp \sqrt{1 + \sin^2(\alpha + 2k\pi/L)}]e^{i(\pi(\varphi_p - \varphi_q)/2 - 2k\pi/L)}$ .

The spectrum is degenerate whenever for different  $k, l$  we have  $\cos(\alpha + 2k\pi/L) = \cos(\alpha + 2l\pi/L)$  which happens whenever  $\alpha$  is an integer multiple of  $\pi/L$ . Then (almost) every invariant space is two-dimensional and a variety of bases other than Bloch functions is allowed. This non-generic case happens for instance for the most common choices of phases ( $\varphi_q = \varphi_p = 0$  or  $1/2$ ). The quasi-energy spectrum of the closed regular multibaker for the phases  $\varphi_q = \varphi_p = 1/2$  is shown in Figure 3.

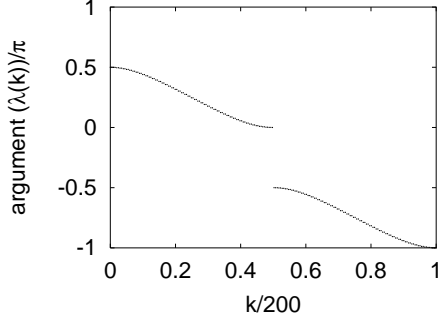


FIG. 3: Eigenspectrum of the closed regular quantum multi-baker for the chain of length  $L = 101$  cells with periodic boundary conditions. Phases are  $\varphi_q = \varphi_p = 1/2$ ,  $\alpha = \pi$ ,  $\beta = 3\pi/4$ .

### B. Open case: absorbing boundary conditions

Next we consider the regular quantum multi-baker, still for  $N = 2$ , but with open boundaries. In the classical case, open boundaries are important for the application of the escape-rate formalism of Gaspard and Nicolis [29] which relates the rate of decay of the initial number of particles on a large, open chain to the diffusion coefficient, and then to the Lyapunov exponents and the Kolmogorov-Sinai entropy of trajectories on a fractal repeller, *i.e.* the set of initial points for trajectories that never leave the chain [4, 30]. It is of some interest, then, to contrast the classical and quantum cases.

We take the multi-baker dynamics given by (19) in the cells  $n = 1, 2, \dots, L - 2$ . At the boundary cells we allow the probability density to escape from the right half cell for  $n = 0$ , and from the left half cell for  $n = L - 1$ , and nothing enters the system from the outside. The latter condition requires

$$\Psi_b(0, t) = 0, \quad (29)$$

$$\Psi_t(L - 1, t) = 0. \quad (30)$$

Due to the escape of probability density, the eigenvalues that determine the time dependence of the probability density in each cell move to the interior of the unit circle. A simple proof of this fact is given in Appendix A. We show there also that the kernel is two-dimensional.

To determine the non-zero eigenvalues  $0 < |\lambda| < 1$  of the open chain, we first write the eigenvalue equation in the momentum representation. Then every eigenstate  $\Psi$  satisfies the equation

$$\begin{bmatrix} \tilde{\Psi}_b(n+1) \\ \tilde{\Psi}_t(n-1) \end{bmatrix} = \begin{bmatrix} f_0/\lambda & 0 \\ 0 & f_0/\lambda \end{bmatrix} \cdot G_2^{-1}(\varphi_q, \varphi_p) \cdot \begin{bmatrix} \tilde{\Psi}_b(n) \\ \tilde{\Psi}_t(n) \end{bmatrix}. \quad (31)$$

Viewed in terms of the “top” and “bottom” states, we see that the solution of Eq. (31) can be neatly formulated as a scattering problem (see Figure 4), where the incoming waves are  $\tilde{\Psi}_b(n)$  and  $\tilde{\Psi}_t(n)$ , and the outgoing

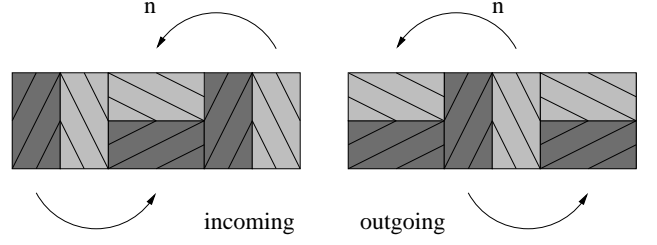


FIG. 4: Scattering from one cell.

waves are  $\tilde{\Psi}_b(n+1)$  and  $\tilde{\Psi}_t(n-1)$  with a one-cell scattering  $S$ -matrix, and a one-cell transfer  $T$ -matrix. Those are defined, respectively, by the relations

$$\begin{bmatrix} \tilde{\Psi}_t(n-1) \\ \tilde{\Psi}_b(n+1) \end{bmatrix} = S \cdot \begin{bmatrix} \tilde{\Psi}_b(n) \\ \tilde{\Psi}_t(n) \end{bmatrix}, \quad (32)$$

and

$$\begin{bmatrix} \tilde{\Psi}_b(n+1) \\ \tilde{\Psi}_t(n) \end{bmatrix} = T \cdot \begin{bmatrix} \tilde{\Psi}_b(n) \\ \tilde{\Psi}_t(n-1) \end{bmatrix}. \quad (33)$$

Explicitly, the  $S$ -matrix is, for the regular multi-baker, given

$$S = \begin{bmatrix} \frac{1}{\sqrt{2}} e^{i\pi\varphi_p(1-\varphi_q)/\lambda} & \frac{1}{\sqrt{2}} e^{i\pi(1+\varphi_q+\varphi_p-\varphi_q\varphi_p)/\lambda} \\ \frac{1}{\sqrt{2}} e^{-i\pi\varphi_q\varphi_p/\lambda} & \frac{1}{\sqrt{2}} e^{i\pi\varphi_q(1-\varphi_p)/\lambda} \end{bmatrix}, \quad (34)$$

and the  $T$ -matrix is

$$T = \begin{bmatrix} \sqrt{2} e^{-i\pi\varphi_q\varphi_p/\lambda} & -e^{-i\pi\varphi_p} \\ e^{-i\pi\varphi_q} & \sqrt{2} e^{-i\pi(1+\varphi_q+\varphi_p-\varphi_q\varphi_p)/\lambda} \end{bmatrix}. \quad (35)$$

We find it convenient to use the transfer operators,  $T$ , to carry out the determination of the eigenvalues,  $\lambda$ , governing the rate of decay for an open system. To do this we first use the transfer operators to relate the quantum states at one end of the chain to the states at the other end, and then use the open, absorbing boundary conditions to obtain an explicit equation for  $\lambda$ . First, the states at the two ends of the chain are related by

$$\begin{bmatrix} \tilde{\Psi}_b(L-1) \\ \tilde{\Psi}_t(L-2) \end{bmatrix} = T^{L-2} \cdot \begin{bmatrix} \tilde{\Psi}_b(1) \\ \tilde{\Psi}_t(0) \end{bmatrix}. \quad (36)$$

To use the boundary conditions, we first look at cell  $L-1$ . We note that in the open multi-baker  $\tilde{\Psi}_t(L-1) = 0$ . Then using Eq. (31), we obtain  $\tilde{\Psi}_t(L-2) = (f_0/\lambda)[g_{10}\tilde{\Psi}_b(L-1) + g_{11}\tilde{\Psi}_t(L-1)]$ , and  $\tilde{\Psi}_t(L-1) = [(\lambda/f_0)\tilde{\Psi}_t(L-2) - g_{10}\tilde{\Psi}_b(L-1)]/g_{11}$ . Thus

$$0 = \begin{bmatrix} -g_{10} & (\lambda/f_0) \end{bmatrix} \cdot \begin{bmatrix} \tilde{\Psi}_b(L-1) \\ \tilde{\Psi}_t(L-2) \end{bmatrix}. \quad (37)$$

Using Eq. (32) and (36), we easily find that  $\tilde{\Psi}_b(1) = (f_0 g_{01}/\lambda)\tilde{\Psi}_t(0)$ . Thus the equation that determines the decay rates is

$$0 = \begin{bmatrix} -f_0 g_{10} & \lambda \end{bmatrix} \cdot T^{L-2} \cdot \begin{bmatrix} f_0 g_{01} \\ \lambda \end{bmatrix}, \quad (38)$$

where a scalar product of matrices is to be taken as indicated. To get a useful form for this equation we need to find the eigenvalues of the transfer matrix  $T$ . We denote the eigenvalues of  $T$  by  $\chi_+, \chi_-$ , which are obtained as solutions of the quadratic equation

$$\chi e^{i\alpha} + \frac{1}{\chi e^{i\alpha}} = \sqrt{2}[\lambda/e^{i\beta} + e^{i\beta}/\lambda], \quad (39)$$

where  $\alpha, \beta$  are given by Eq. (25). Using, as before, the notation  $u = \chi e^{i\alpha}$ ,  $v = \lambda/e^{i\beta}$  we obtain the same formal relation between  $u$  and  $v$  as in the periodic case, Eq. (27), *i.e.*

$$v + \frac{1}{v} = \frac{1}{\sqrt{2}} \left[ u + \frac{1}{u} \right], \quad (40)$$

The two solutions  $u_+, u_-$  satisfy  $u_+ u_- = 1$ , and  $u_+ + u_- = \sqrt{2}[v + 1/v]$ . Since  $|v| = |\lambda| < 1$ , it follows that  $u_+, u_-$  do not lie on the unit circle. In particular, they must be different and so the matrix  $T$  is non-degenerate. We take  $|u_+| > 1 > |u_-|$  to define them uniquely, and use  $u_{\pm} = \chi_{\pm} e^{i\alpha}$ . If we set  $u_{\pm} = e^{\pm i\kappa}$ , and then solve for  $v$  we obtain

$$v_{\pm} = \frac{1}{\sqrt{2}} [\cos \kappa \pm i \sqrt{1 + \sin^2 \kappa}]. \quad (41)$$

We look for solutions where  $\kappa$  is not purely real, that is,  $\kappa \in \mathbb{C} \setminus \mathbb{R}$ . We next use a simple identity for the  $L$ -th power of non-degenerate matrix  $T$ , given by

$$\begin{aligned} T^L &= \frac{\chi_+^L - \chi_-^L}{\chi_+ - \chi_-} T - \frac{\chi_+^L - \chi_-^L}{\chi_+ - \chi_-} I \\ &= \frac{e^{-i\alpha(L-1)}}{\sin \kappa} [\sin(L\kappa) T - \sin((L-1)\kappa) I], \end{aligned}$$

to write Eq. (38) in the form

$$\left[ 2v^2 + 2 + \frac{1}{v^2} \right] \sin(L-2)\kappa = \left[ \sqrt{2}v + \frac{1}{\sqrt{2}v} \right] \sin(L-3)\kappa, \quad (42)$$

where  $v$  is one of  $v_{\pm}$ . With the help of (40) and (41) we can reduce (42) to

$$\sin L\kappa + \sin \kappa \cos(L-1)\kappa + i\varepsilon \sqrt{1 + \sin^2 \kappa} \sin(L-1)\kappa = 0, \quad (43)$$

which can be further reduced to

$$u^{2L} - 1 - 2 \sin \kappa [\sin \kappa - \varepsilon \sqrt{1 + \sin^2 \kappa}] = 0. \quad (44)$$

In the above equations  $\varepsilon = \pm 1$  corresponds to the sign in (41). Clearly, we can get all of the possible solutions multiplying Eq. (44) for two different signs. This leads to a very simple equation

$$\sin^2 L\kappa + \sin^2 \kappa = 0. \quad (45)$$

The only real solutions of this equation are  $\kappa = k\pi$ ,  $k \in \mathbb{Z}$ , but, as mentioned above, they must be discarded. If we write Eq. (45) as

$$\sin L\kappa = i\delta \sin \kappa, \quad (46)$$

where  $\delta = \pm 1$ , we can treat it as a “perturbation” in  $\delta$  of equation  $\sin L\kappa = 0$  [31]. Thus we can obtain the solutions of interest by expanding  $\kappa$  in powers of  $\delta$  about the values  $\kappa = k\pi/L$ ,  $k = 1, \dots, L-1$ , [36] and then at the end, setting  $\delta = \pm 1$ . This approach gives results which quickly converge numerically, for all allowed values of  $k$ . To apply this procedure it is convenient to rewrite Eq. (46) in a polynomial representation,

$$u^{2L} - 1 - \delta i u^L (u - 1/u) = 0. \quad (47)$$

Then, by taking  $u = \exp(i(k\pi/L + \delta a_1 + \delta^2 a_2 + \dots))$ , one can determine the coefficients  $a_i$ , and check the convergence of the series numerically. Figure 5 shows the

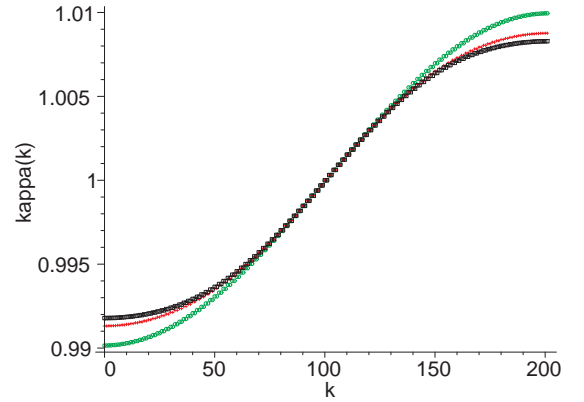


FIG. 5: The first and the fifth order approximate solutions and the numerical solutions of Eq. (46) for  $L = 101$ . We took here  $\delta = 1$ . The numerical solution is the middle curve. Fifth order approximate solution is the one closer to the numerical solution.

absolute values of the approximate solutions (in the first and fifth order) and the numerical solutions for  $L = 101$  sorted according to increasing amplitude. The first few coefficients in the expansion of  $u$  are

$$\begin{aligned} a_1 &= -b/L, \\ a_2 &= -iab/L^2, \\ a_3 &= b^3/6L + b(2 - 3b^2)/2L^3, \\ a_4 &= i(2ab^3/3L^2 - ab(8b^2 - 3)/3L^4), \end{aligned}$$

where

$$a = \cos(k\pi/L), \quad b = \sin(k\pi/L). \quad (48)$$

Numerical studies show rapid convergence of amplitudes and slower convergence of phases.

Next we calculate the approximate eigenvalues of the open quantum multibaker. Using  $\lambda = e^{i\beta}v$ , keeping  $|v| < 1$  solutions, to second order in  $\delta$  we obtain



$$\lambda = \frac{e^{i\beta}}{\sqrt{2}} \left( a + i\varepsilon \sqrt{1+b^2} \right) \exp \left\{ -\frac{b^2}{L \sqrt{1+b^2}} \right\} \exp \left\{ -\frac{i\varepsilon ab^2 (2b^2+3)}{2L^2 (1+b^2)^{3/2}} \right\}, \quad (49)$$

where  $a, b$  are given by (48), while  $\varepsilon = \pm 1$  enumerates the solutions. The non-exponential factor on the right hand side is the unperturbed solution. Figure IV B shows the absolute value of  $v$  (in the fourth order approximation).

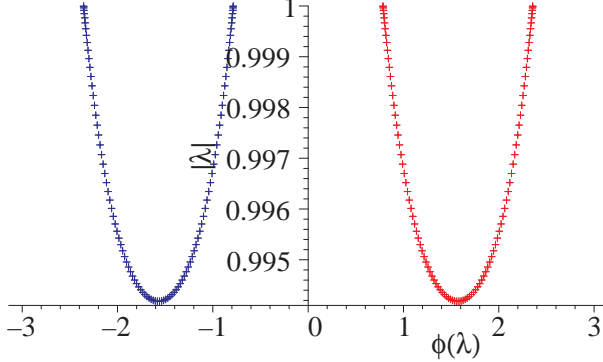


FIG. 6: The amplitude versus argument of  $\lambda$  in the fourth order of approximation for the chain of length  $L = 101$ .

The general result and the numerical studies suggest that the value of  $v$  that is the nearest to the unit circle occurs when  $k$  takes on one of the four values,  $k \in \{1, L-1, L+1, 2L-1\}$ . To get the leading term in the large-size limit we find it convenient to use an alternative expansion of Eq. (46), in powers of  $L^{-1}$ . While this leads to an asymptotic solution for  $v$  which quickly diverges for most  $k$ , it gives us the correct leading order behavior for  $k \ll L$ . Then the expansion of the solution of Eq. (46) in powers of  $1/L$ , as  $\kappa_k = k\pi/L + b_2/L^2 + b_3/L^3 + \dots$  for small  $k$  yields

$$\kappa_k \approx k\pi(1/L + i\delta/L^2 - 1/L^3 - i\delta(1 + k^2\pi^2/3)/L^4 + \dots), \quad (50)$$

which gives the asymptotic formula for  $v(k)$

$$v(k) = \frac{1}{\sqrt{2}} [\cos \kappa_k \pm i \sqrt{1 + \sin^2(\kappa_k)}] \quad (51)$$

$$\approx \exp \left[ \pm i \left( \frac{\pi}{4} + \frac{k^2\pi^2}{2L^2} \right) \right] \exp \frac{-k^2\pi^2}{L^3}. \quad (52)$$

The escape of probability density from the open regular quantum multibaker is governed by the escape rate

$$\gamma := -\lim_{t \rightarrow \infty} \frac{\log P(t)}{t} \quad (53)$$

which is approximately

$$\gamma = -\log |v(1)|^2 \approx \frac{2\pi^2}{L^3}. \quad (54)$$

Therefore, even though the motion *inside* the quantum multibaker is *faster* (ballistic) than in the corresponding classical system (diffusive), the *effusion* (decay of probability density) is *slower* than that for the corresponding classical system, ([4]; see also Section II B)

$$\gamma_{\text{class}} = \frac{\pi^2}{2L^2}. \quad (55)$$

We also mention here that in their study of scattering resonances for an open, periodic chain of scatterers, Barra and Gaspard [28] found a  $1/L$  decay of the corresponding escape-rate. The difference between the results found here and those of Barra and Gaspard is due to the differences in the two models of the reflection and transmission coefficients at each site. For the multibaker case, these coefficients are fixed constants, while Barra and Gaspard consider models where the reflection coefficients scale as the inverse of the energy of the particle, and the authors consider the high energy case. Evidently, for the long wavelength case,  $N = 2$ , the particle has some difficulty finding the exit channels, while for small enough wavelengths, as considered in Ref. [28], the particle finds the exit channels more easily. Note that the logarithms of the fastest decaying eigenvalues, both for our system and for the systems considered by Barra and Gaspard, scale as  $1/L$ .

### C. Steady state solution

Suppose now that the multibaker of length  $L$  is connected at both ends to infinitely conducting leads. We suppose that there can be traveling waves in the leads moving to the right and to the left. These waves are most conveniently described in terms of the momentum space representation of the wave functions, and we recall that the “bottom” states come from the left and the “top” states come from the right. Thus to the left of the chain,  $n < 0$ , we take the traveling waves to be

$$\tilde{\Psi}_b(n, t) = A e^{i(\omega t - kn)}, \quad (56)$$

$$\tilde{\Psi}_t(n, t) = B e^{i(\omega t + kn)}, \quad (57)$$

and to the right of the chain,  $n > L-1$ , the waves are

$$\tilde{\Psi}_b(n, t) = C e^{i(\omega t - kn)}, \quad (58)$$

$$\tilde{\Psi}_t(n, t) = D e^{i(\omega t + kn)}. \quad (59)$$

Here  $A, D$  are the amplitudes of the incoming waves, while  $B, C$  are the amplitudes of the outgoing waves.

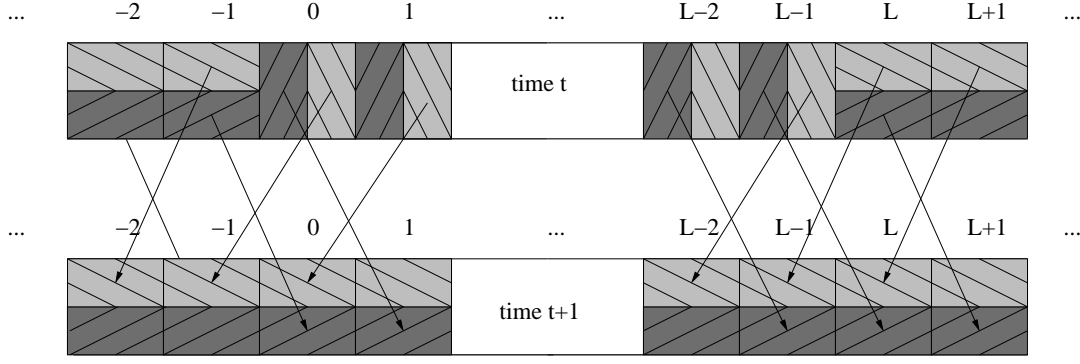


FIG. 7: Scattering from a quantum multibaker.

Due to the dynamics on the multibaker, we can match the incoming wave functions in the leads to the proper momentum space functions for the unit cells at 0 and at  $L-1$ . This matching condition is simply

$$\tilde{\Psi}_b(0, t) = Ae^{i\omega t}, \quad (60)$$

$$\tilde{\Psi}_t(L-1, t) = De^{i\omega t} e^{i(L-1)k}. \quad (61)$$

We will use a scattering approach to find the outgoing amplitudes,  $B, C$  for the steady state solution, as well as to solve the problem of the relaxation of some initial state to a steady state. First we consider the steady state solution for the baker chain with conducting leads.

The steady state solution is defined by the condition that the time dependence of the wave function can be incorporated in a time dependent phase factor. Since the dynamics takes place at discrete times, we suppose that, for example,  $\Psi_{t,b}(n, t+1) = e^{i\tilde{\omega}} \Psi_{t,b}(n, t)$  implies  $\Psi_{t,b}(n, t) = e^{i\tilde{\omega}t} \Psi_{t,b}(n, 0)$ . In particular, using Eq. (60),  $\Psi_b(0, t) = e^{i\tilde{\omega}t} \Psi_b(0, 0)$ , so that  $\tilde{\omega} \equiv \omega$ . Writing  $\tilde{\Psi}_b(n, t) = e^{i\omega t} \tilde{\Psi}_b(n)$ , etc., we obtain the steady state equation

$$\begin{bmatrix} \tilde{\Psi}_b(n+1) \\ \tilde{\Psi}_t(n-1) \end{bmatrix} = \begin{bmatrix} f_0 e^{-i\omega} & 0 \\ 0 & f_0 e^{-i\omega} \end{bmatrix} \begin{bmatrix} \Psi_l(n) \\ \Psi_r(n) \end{bmatrix}. \quad (62)$$

The transmission and reflection coefficients for the chain can be expressed in terms of the scattering  $S$ -matrix, given by

$$\begin{bmatrix} \tilde{\Psi}_t(-1) \\ \tilde{\Psi}_b(L) \end{bmatrix} = S_{0,L-1} \begin{bmatrix} \tilde{\Psi}_b(0) \\ \tilde{\Psi}_t(L-1) \end{bmatrix}, \quad (63)$$

where the elements of  $S$ -matrix are

$$S_{0,L-1} = \begin{bmatrix} r_{0,L-1} & t'_{0,L-1} \\ t_{0,L-1} & r'_{0,L-1} \end{bmatrix}. \quad (64)$$

Here the unprimed coefficients refer to waves incident on the left end of the chain, while the primed quantities refer to the waves incident on the right side of the chain. The transmission and reflection coefficients,  $T, T', R, R'$  respectively, are then obtained from the elements of  $S$  by

$$T = |t_{0,L-1}|^2, \quad R = |r_{0,L-1}|^2, \quad (65)$$

and similarly for the primed quantities. Unitarity of  $S$  implies  $T = T', R = R'$ . In order to calculate the  $S$ -matrix,  $S_{0,L-1}$ , for the chain, we proceed as for the absorbing case, by looking at the transfer and scattering matrices for one cell, and building up the matrices for the chain by iteration, cell by cell. Consider the cell labelled by the index  $n$ . The  $S$ -matrix for the  $n$ -th cell is given by

$$\begin{bmatrix} \tilde{\Psi}_t(n-1) \\ \tilde{\Psi}_b(n+1) \end{bmatrix} = S_n \begin{bmatrix} \tilde{\Psi}_b(n) \\ \tilde{\Psi}_t(n) \end{bmatrix}, \quad (66)$$

and the transfer  $T$ -matrix is

$$\begin{bmatrix} \tilde{\Psi}_b(n+1) \\ \tilde{\Psi}_t(n) \end{bmatrix} = T_n \begin{bmatrix} \tilde{\Psi}_b(n) \\ \tilde{\Psi}_t(n-1) \end{bmatrix}. \quad (67)$$

Each of the matrices can be given in terms of the other, thus,

$$S = \begin{bmatrix} r & t' \\ t & r' \end{bmatrix} \Rightarrow T = \begin{bmatrix} t - r't'^{-1}r & r't'^{-1} \\ -t'^{-1}r & t'^{-1} \end{bmatrix}, \quad (68)$$

$$T = \begin{bmatrix} \alpha & \gamma \\ \beta & \delta \end{bmatrix} \Rightarrow S = \begin{bmatrix} -\delta^{-1}\beta & \delta^{-1} \\ \alpha - \gamma\delta^{-1}\beta & \gamma\delta^{-1} \end{bmatrix}. \quad (69)$$

The  $S$  and  $T$  matrices can easily be obtained by transforming the dynamical equations (62) to momentum representation (18), so that

$$\begin{bmatrix} \tilde{\Psi}_b(n+1) \\ \tilde{\Psi}_t(n-1) \end{bmatrix} = f_0 e^{-i\omega} \begin{bmatrix} g_{00} & g_{01} \\ g_{10} & g_{11} \end{bmatrix} \begin{bmatrix} \tilde{\Psi}_b(n) \\ \tilde{\Psi}_t(n) \end{bmatrix}, \quad (70)$$

from which the  $S$ -matrix follows as

$$S_n = \frac{e^{-i\omega}}{\sqrt{2}} \begin{bmatrix} e^{i\pi\varphi_p(1-\varphi_q)} & e^{i\pi(1+\varphi_q+\varphi_p-\varphi_q\varphi_p)} \\ e^{-i\pi\varphi_q\varphi_p} & e^{i\pi\varphi_q(1-\varphi_p)} \end{bmatrix}. \quad (71)$$

The  $T$ -matrix is then given by

$$T_n = \begin{bmatrix} \sqrt{2}e^{-i\omega}e^{-i\pi\varphi_q\varphi_p} & -e^{-i\pi\varphi_p} \\ e^{-i\pi\varphi_q} & \sqrt{2}e^{i\omega}e^{-i\pi(1+\varphi_q+\varphi_p-\varphi_q\varphi_p)} \end{bmatrix}. \quad (72)$$

The scattering matrix for the whole multibaker  $S_{0,L-1}$  can easily be derived from  $T_{0,L-1} := T_{L-1} \cdot \dots \cdot T_1 \cdot T_0$ . Its unitarity can also be verified. For the regular system

$$T_{0,L-1} = T^L = \frac{\chi_+^L - \chi_-^L}{\chi_+ - \chi_-} T - \frac{\chi_- \chi_+^L - \chi_+ \chi_-^L}{\chi_+ - \chi_-} \quad (73)$$

where  $\chi_{\pm}$  are roots of characteristic polynomial of  $T$

$$\chi_{\pm} = e^{-i\alpha} [\sqrt{2} \cos(\beta - \omega) \pm \sqrt{\cos 2(\beta - \omega)}], \quad (74)$$

and  $\alpha, \beta$  are given by Eq. (25). Depending on the sign of  $\cos 2(\beta - \omega)$  there are two types of solutions: if the frequency of the incident wave falls in one of the quasi-energy bands

$$\cos 2(\beta - \omega) < 0 \Leftrightarrow \omega - \beta \in [\pi/4, 3\pi/4] \cup [5\pi/4, 7\pi/4], \quad (75)$$

we have the oscillatory case with some interesting structure. Otherwise, when the frequency of the incident wave falls in the gap, we observe almost total reflection of particles coming from the leads to the chain, becoming total as  $L \rightarrow \infty$  (the exponential case).

1. If  $\cos 2(\beta - \omega) < 0$  (oscillatory case), the characteristic roots are:

$$\chi_{\pm} = e^{-i\alpha} [\sqrt{2} \cos(\beta - \omega) \pm i \sqrt{-\cos 2(\beta - \omega)}], \quad (76)$$

thus  $|\chi_{\pm}|^2 = 1$ . Set  $\chi_{\pm} = e^{-i\alpha} e^{\pm i\kappa}$ . Then the transmission and reflection coefficients are

$$R = \frac{\sin^2 L\kappa}{\sin^2 \kappa + \sin^2 L\kappa} = \frac{1}{1 + \frac{\sin^2 \kappa}{\sin^2 L\kappa}}, \quad (77)$$

$$T = \frac{\sin^2 \kappa}{\sin^2 \kappa + \sin^2 L\kappa} = \frac{1}{1 + \frac{\sin^2 L\kappa}{\sin^2 \kappa}}. \quad (78)$$

Some interesting special cases occur when:

$$(a) \kappa = k\pi + \pi/2, L \text{ odd: } T = 1/2;$$

$$(b) \kappa = k\pi + \pi/2, L \text{ even: } T = 1;$$

$$(c) \kappa = k\pi: T = 1/(1 + L^2);$$

$$(d) \kappa = k\pi/L: T = 1.$$

We will refer to the cases when  $T = 1$  as resonances.

2. In the exponential case, when  $\cos 2(\beta - \omega) > 0$ , we have  $|\chi_{\pm}|^2 \geq 1$ , and  $\chi_+ \chi_-^* = 1$ , so that  $|\chi_-| = \frac{1}{|\chi_+|}$ . Then the transmission and reflection coefficients are

$$R = \frac{(|\chi_+|^L - |\chi_-|^L)^2}{(|\chi_+|^L - |\chi_-|^L)^2 + (|\chi_+| - |\chi_-|)^2} \quad (79)$$

$$\approx 1 - |\chi_-|^{2(L-1)} \approx 1 \quad (80)$$

$$T = \frac{(|\chi_+| - |\chi_-|)^2}{(|\chi_+|^L - |\chi_-|^L)^2 + (|\chi_+| - |\chi_-|)^2} \quad (81)$$

$$\approx |\chi_-|^{2(L-1)} \approx 0. \quad (82)$$

#### D. Density profile in the steady state — violation of the Fick's law

As mentioned above, the oscillatory case provides some interesting structures, illustrating the interference between waves traveling to the right and left along the chain. The algebra is tedious but straightforward, and we don't reproduce it here, merely stating the final results.

The wave function in the steady state is

$$\begin{aligned} \Psi_b(n) &= \frac{e^{-i\alpha n}}{z_L} [z_{L-n} \Psi_b(0) - e^{i\alpha L} e^{i(\alpha - \pi\varphi_p)} \sin n\kappa \Psi_t(L-1)], \\ \Psi_t(n) &= \frac{e^{-i\alpha(n+1-L)}}{z_L} [e^{-i\alpha L} e^{i(\alpha - \pi\varphi_q)} \sin \kappa(n+1-L) \Psi_b(0) + z_{n+1} \Psi_t(L-1)]. \end{aligned}$$

We introduce the probability densities,  $\varrho_L$  and  $\varrho_R$  from the left and right leads, respectively, in terms of the corresponding wave functions, by writing  $\Psi_b(0) = \sqrt{\varrho_L}$ ,  $\Psi_t(L-1) = \sqrt{\varrho_R} e^{i\eta}$ , where  $\eta$  denotes a relative phase between the wave functions at the two ends. To simplify the formulas we introduce

$$z_n \equiv r_n e^{i\varphi_n} := \sqrt{2} \sin n\kappa e^{-i(\beta - \omega)} - \sin \kappa(n-1)$$

$$= \cos \kappa n \sin \kappa - i\varepsilon \sin n\kappa \sqrt{1 + \sin^2 \kappa},$$

where  $\varepsilon = \pm$  is the sign of  $\sin(\beta - \omega)$ . Then, introducing the angle  $\varphi = \pi(\varphi_q - \varphi_p)/2 + \alpha L + \eta$ , we obtain the total probability density at cell  $n$

$$\varrho(n) = \frac{\sin^2(L-n-1)\kappa + \sin^2(L-n)\kappa + \sin^2\kappa}{|z_L|^2} \varrho_L + \frac{\sin^2\kappa n + \sin^2\kappa(n+1) + \sin^2\kappa}{|z_L|^2} \varrho_R - i \frac{\sqrt{\varrho_L \varrho_R}}{|z_L|^2} \left\{ \sin(L-1-n)\kappa [z_{n+1} e^{i\varphi} - z_{n+1}^* e^{-i\varphi}] - \sin n\kappa [z_{L-n}^* e^{i\varphi} - z_{L-n} e^{-i\varphi}] \right\}.$$

At resonance ( $\kappa = k\pi/L$ ) it takes form

$$\varrho(n) = \left( 1 + \frac{\sin^2\kappa n + \sin^2\kappa(n+1)}{\sin^2\kappa} \right) (\varrho_L + \varrho_R) + 2 \frac{\sqrt{\varrho_L \varrho_R}}{\sin\kappa} r_{2n+1} \sin(\varphi + \varphi_{2n+1}). \quad (83)$$

Let us concentrate on this last expression, for simplicity. Since  $|z_n|^2 = \sin^2\kappa + \sin^2 n\kappa$ , then if we write  $\varrho(n) = \varrho_1(n)(\varrho_L + \varrho_R) + 2\varrho_2(n)\sqrt{\varrho_L \varrho_R}$ , then  $0 \leq \frac{|\varrho_2|}{\varrho_1} \frac{2\sqrt{\varrho_L \varrho_R}}{\varrho_L + \varrho_R} \leq 1$ , which implies, in particular, positivity of  $\varrho$ . For small  $k$  it turns out that the second term is negligible (Figure 8). We can easily estimate the behavior of the probability density profile in this case. For large  $L$  and small  $k$  we have

$$\varrho_k(n) \approx \left( 1 + \frac{1 - \cos k\pi/L}{k^2\pi^2/L^2} \cos \frac{k\pi(2n+1)}{L} \right) (\varrho_L + \varrho_R), \quad (84)$$

which for  $k = 1$  can also be approximated as  $\varrho(n) \approx \left( 1 + \frac{2L^2}{\pi^2} \sin \frac{\pi}{L} (n + \frac{1}{2}) \right) (\varrho_L + \varrho_R)$ . Figure 8 shows the approximate solution (crosses) and the full solution (diamonds) as well as the probability density of the bottom states (boxes) and the top states (circles). For the smallest resonance ( $k = 1$ ) the probability distribution achieves maximum around  $n = L/2$  where it is approximately  $2L^2/\pi^2$ .

These results are clearly connected to the slow probability escape  $\propto 1/L^3$ . To understand them consider a plane wave coming from the left with a resonant frequency going through the open quantum multibaker. Thus at every time step we inject the same density inside. The wave travels ballistically inside and when it reaches the end is mostly reflected, partially transmitted. Due to the fast motion inside and slow decay the density accumulates in the multibaker and reaches the steady state when the escape on the right balanced the injection on the left. The probability density of the resulting standing wave is given by Eq. (83).

This result is very striking in comparison with the classical case: in the classical multibaker one obtains Fick's behavior [4, 8, 9] — there is a linear profile of probability density. This is also what happens for partially integrated classical dynamics which we considered in section II C. In particular, the probability density at any point inside the multibaker is between the densities of the reservoirs.

We defer the complete discussion of the steady state solutions to a further work where it will be considered

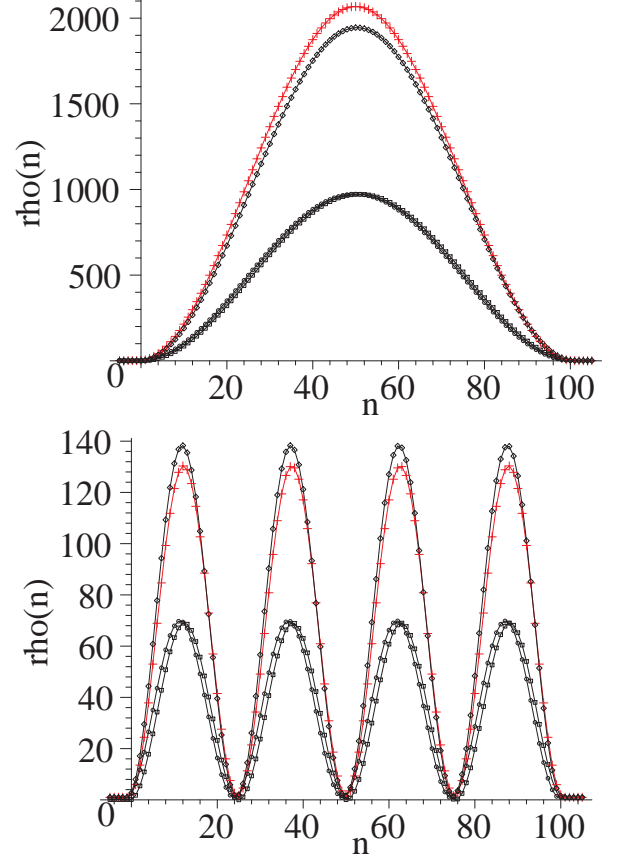


FIG. 8: Profile of the probability density in the steady state for the smallest and the fourth resonances  $\kappa = k\pi/L$  with  $k = 1, 4$ . Crosses show the approximate solution, diamonds stand for the full solution. Also shown is the probability density of the bottom (boxes) and the top states (circles). We took  $\varrho_L = 0.1$ ,  $\varrho_R = 0.9$ ,  $\eta = 0$ . The horizontal axis range is  $[-5, 105]$ .

together with the semi-classical case in the context of transport [21]. Here let us only mention that the approach to the steady state can be conveniently studied as a spectral problem: The evolution equations for the quantum multibaker with two waves scattering from left and right can be written as

$$\hat{\Psi}(t) = \hat{B}_L \hat{\Psi}(t-1) + \Phi_0, \quad (85)$$

where  $\hat{\Psi}(t) := e^{-i\omega t} \Psi(t)$ ,  $\hat{B}_L$  is the matrix representation of the open multibaker propagator following from

the equations

$$\begin{bmatrix} \hat{\Psi}_l(n, t) \\ \hat{\Psi}_r(n, t) \end{bmatrix} = G_2^{-1} \cdot \begin{bmatrix} f_0 e^{-i\omega} & 0 \\ 0 & f_0 e^{-i\omega} \end{bmatrix} \begin{bmatrix} \hat{\Psi}_l(n-1, t) \\ \hat{\Psi}_r(n+1, t) \end{bmatrix}, \quad (86)$$

and  $\Phi_0$  denotes the steady state boundary conditions:  $\Phi_0 = [\Phi_b(0), \Phi_t(0), \dots, \Phi_b(L-1), \Phi_t(L-1)]^T$ ,  $\Phi_b(0) = A$ ,  $\Phi_t(L-1) = D e^{ik(L-1)}$ ,  $\Phi_{b,t}(n) = 0$  otherwise. The solution to this simple affine problem is

$$|\hat{\Psi}(t)\rangle = \sum_{\lambda_k} \frac{1 - \lambda_k^t}{1 - \lambda_k} |\varphi_k\rangle \langle \varphi_k | \Phi_0 \rangle + \sum_{\lambda_k} \lambda_k^t |\varphi_k\rangle \langle \varphi_k | \hat{\Psi}(0) \rangle, \quad (87)$$

where  $\lambda_k$  are the  $\omega$ -dependent eigenvalues of  $\hat{B}_L$  and the  $|\varphi_k\rangle$  are the corresponding eigenvectors. In particular, if at time 0 the system is empty  $\Psi(0) = 0$ , then the solution is

$$|\hat{\Psi}(t)\rangle = \sum_{\lambda_k} \frac{1 - \lambda_k^t}{1 - \lambda_k} |\varphi_k\rangle \langle \varphi_k | \Phi_0 \rangle. \quad (88)$$

The steady state is the time invariant part of the above solution

$$|\hat{\Psi}\rangle = \sum_{\lambda_k} \frac{1}{1 - \lambda_k} |\varphi_k\rangle \langle \varphi_k | \Phi_0 \rangle. \quad (89)$$

The approach to the steady state is given by the eigenvalues of the open multibaker (49), thus it is as slow as the escape of probability density, which is consistent with the accumulation of large probability density in the system. Note that the distribution of the absolute values of the eigenvalues of  $\hat{B}_L$  is  $\omega$  independent, yet the steady state solution does depend on  $\omega$ .

## V. THE CLOSED RANDOM QUANTUM MULTIBAKER FOR $N = 2$

In this section we extend our discussion of the quantum multibaker map for  $N = 2$  by considering the case where the phases,  $\varphi_{q,p}$ , defining the map vary randomly from cell to cell. As expected, the random case differs considerably from the regular case, since the randomness of the phases acts as a disordering mechanism producing a localization of the wave function. Unlike the regular case, there is little that can be done analytically for the random case, other than making use of some known results for the properties of products of random  $2 \times 2$  matrices [32], which in this case are only of limited utility. For this reason we limit ourselves to a presentation of the results of numerical studies.

The random quantum multibaker map is, for the case  $N = 2$ , is defined by the equations

$$\begin{aligned} \Psi_l(n, t+1) &= g_{00}(n) f_0(n-1) \Psi_l(n-1, t) \\ &\quad + g_{01}(n) f_0(n+1) \Psi_r(n+1, t), \\ \Psi_r(n, t+1) &= g_{10}(n) f_0(n-1) \Psi_l(n-1, t) \\ &\quad + g_{11}(n) f_0(n+1) \Psi_r(n+1, t), \end{aligned}$$

where the phases in each of the cells are drawn randomly from some distribution. Here we use a uniform distribution of phases in the unit interval.

The numerically obtained quasi-energy spectrum is illustrated in Figure 9 and can be compared with that for the regular case. It can be seen that the eigen-

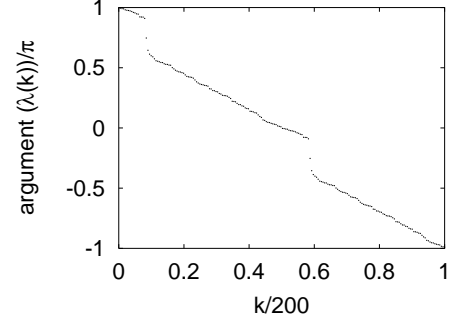


FIG. 9: Spectrum of a the quantum multibaker map for  $L = 101$  cells.

states are localized but the localization does not seem to be purely exponential, as illustrated in Figure 10, where some states are localized over some tens of cells, while others are localized over several times as many cells. The quasi-energies associated with the eigenstates

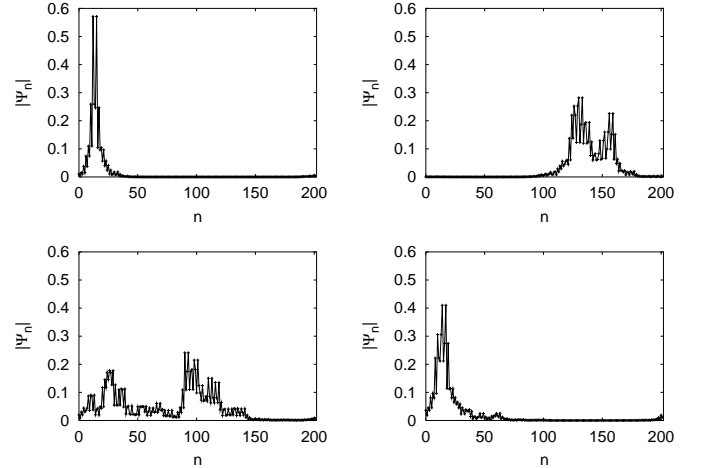


FIG. 10: Four examples out of 202 eigenstates of a realization of the quantum random multibaker of length  $L = 101$  with periodic boundary conditions. Absolute values of  $\Psi_L(n)$ ,  $\Psi_R(n)$  are shown. Notice that  $|\Psi_L(n)| = |\Psi_R(n+1)|$  which results in particular in the twin peak structures.

$\Psi(t) = [\Psi_l(0), \Psi_r(0), \dots, \Psi_l(L-1), \Psi_r(L-1)]$ , are determined by the solution of the following eigenvalue equation,

$$\lambda \begin{bmatrix} \Psi_l(n) \\ \Psi_r(n) \end{bmatrix} = \begin{bmatrix} g_{00}(n) & g_{01}(n) \\ g_{10}(n) & g_{11}(n) \end{bmatrix} \begin{bmatrix} f_0(n-1) \Psi_l(n-1) \\ f_0(n+1) \Psi_r(n+1) \end{bmatrix}, \quad (90)$$

which determines the eigenvalue  $\lambda$ . It is interesting to note that this equation can be put into a form which

shows a close connection between the random quantum multibaker map and a generalized Anderson model for localization (see appendix B). If we define  $\hat{\Psi}(k)$  by

$$\left[ \frac{\lambda g_{10}^*(n+1)}{f_0(n)} - \frac{f_0(n+1)g_{01}(n)}{\lambda} \right] \hat{\Psi}_l(n) = g_{00}(n)g_{10}^*(n+1)\hat{\Psi}_l(n-1) - g_{00}^*(n+1)g_{01}(n)\hat{\Psi}_l(n+1). \quad (91)$$

A similar equation holds for  $\hat{\Psi}_r(n+1)$ . We rewrite this equation so that it takes the form a dynamical problem, where the cell index  $n$  plays the role of the time step. That is,  $\hat{\Psi}_l(n+1) = 2\sqrt{2}e^{i\varphi_1}\sin(\varphi_3)\hat{\Psi}_l(n) - e^{i\varphi_2}\hat{\Psi}_l(n-1)$ , or, using transfer matrices,

$$\begin{bmatrix} \hat{\Psi}_l(n+1) \\ \hat{\Psi}_l(n) \end{bmatrix} = \begin{bmatrix} 2\sqrt{2}e^{i\varphi_1}\sin(\varphi_3) & -e^{i\varphi_2} \\ 1 & 0 \end{bmatrix} \begin{bmatrix} \hat{\Psi}_l(n) \\ \hat{\Psi}_l(n-1) \end{bmatrix}, \quad (92)$$

where the transfer matrix can be written as

$$\begin{bmatrix} e^{i\varphi_1} & 0 \\ 0 & 1 \end{bmatrix} \begin{bmatrix} 2\sqrt{2}\sin(\varphi_3) & -1 \\ 1 & 0 \end{bmatrix} \begin{bmatrix} 1 & 0 \\ 0 & e^{i\varphi_2} \end{bmatrix}. \quad (93)$$

The phases are given by

$$\begin{aligned} \varphi_1 &= (\pi/2)[-1 + \varphi_q(n)\varphi_p(n) - \varphi_q(n+1)\varphi_p(n+1) \\ &\quad - \varphi_q(n) - \varphi_p(n+1)], \\ \varphi_2 &= -\pi(\varphi_q(n) + \varphi_p(n+1) + 1), \\ \varphi_3 &= \kappa + (\pi/2)[\varphi_q(n)\varphi_p(n) + \varphi_q(n+1)\varphi_p(n+1) \\ &\quad - \varphi_q(n) - \varphi_p(n+1)]. \end{aligned}$$

Next, we mention an interesting phenomenon for which we lack a clear explanation at the present time. We first note that the equations connecting  $\hat{\Psi}_l(n)$  with  $\hat{\Psi}_l(n-1)$  and  $\hat{\Psi}_l(n+1)$  involve the same phases and are of the same form as the equation connecting  $\hat{\Psi}_r(n+1)$  with  $\hat{\Psi}_r(n)$  and  $\hat{\Psi}_r(n+2)$ . When the transfer matrix is given by Eq. (93) one can show that the two matrices differ only by two random phases,  $\varphi_1, \varphi_2$ . However, since the equations for  $\hat{\Psi}_l(n)$  and  $\hat{\Psi}_r(n+1)$  separate and have different boundary conditions, there is *a priori* no connection implied between the solutions to the above sets of equations. Indeed, after solving the equations numerically for small  $L$  we find that there is no connection between them. Thus it comes as a surprise that for large  $L$ ,  $|\hat{\Psi}_l(n)| = |\hat{\Psi}_r(n+1)|$ !! This is a numerical result which accounts for the double peaks in Figure 10. To illustrate this unexpected equality, we show several example fragments of eigenstates in Fig. 11. The equality illustrated here is satisfied to within all the allowed precision for  $L > 100$ , and is independent of the shape of the eigenfunction, and remains to be explained.

Finally, we show that the roughly “exponential” shapes of the eigenfunctions can be accounted for in a simple way. From Eq. (92) it follows that  $|\hat{\Psi}_l(n+1)| =$

$\hat{\Psi}_l(k) := f_0(k)\Psi_l(k)$ ,  $\hat{\Psi}_r(k) := f_0(k)\Psi_r(k)$ , we can obtain a set of equations that define a generalized Anderson model:

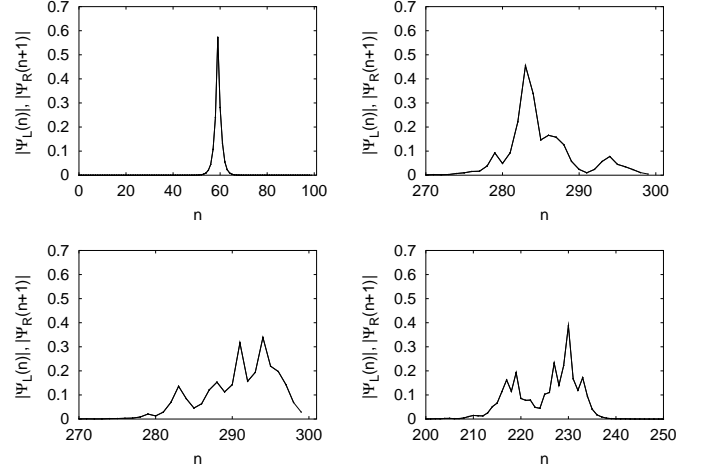


FIG. 11: The figures show plots of *both*  $|\Psi_l(n)|$  and  $|\Psi_r(n+1)|$  superimposed. Fragments of several eigenstates of various realisations of quantum random multibakers were chosen ( $L = 101$  in the first figure,  $L = 301$  in the following figures; the parts not shown are zero within the numerical precision).

$|2\sqrt{2}e^{i(\varphi_1-\varphi_2)}\sin(\varphi_3)\hat{\Psi}_l(n) + \hat{\Psi}_l(n-1)|$ . Thus, on the average we have  $\langle |\hat{\Psi}_l(n+1)|^2 \rangle = 4|\hat{\Psi}_l(n)|^2 + |\hat{\Psi}_l(n-1)|^2$ . Therefore, starting from almost every initial conditions, on the average we should observe growth of  $|\hat{\Psi}_l(n)|^2$  given by  $|\hat{\Psi}_l(n+1)|/|\hat{\Psi}_l(n)| \approx \sqrt{2 + \sqrt{5}} \approx 2.058$ . The numerical distribution of the ratios is given in Figure 12.

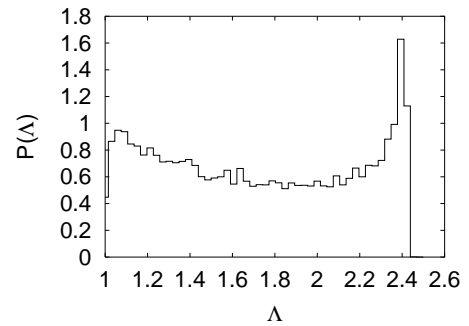


FIG. 12: Distribution of ratios of the succeeding states  $\Lambda := \max\left(\frac{|\hat{\Psi}_l(n+1)|}{|\hat{\Psi}_l(n)|}, \frac{|\hat{\Psi}_l(n)|}{|\hat{\Psi}_l(n+1)|}\right)$  for a set of 202 eigenstates of a realisation of a quantum random multibaker.

This distribution reflects the generally broad distributions associated with the properties of localized states. The difference between the estimated value of the rate of growth with the average obtained from the numerical distribution is due to the contributions from regions where the variation in amplitude from cell to cell is not exponential (compare with Fig. 10).

## VI. SUMMARY OF RESULTS AND DISCUSSION

With this paper we have begun our study of transport properties for quantum multi-baker maps. Our central motivation for this study is, of course, to use a simple, classically chaotic system with transport and entropy production and to explore the differences between the classical system, and its quantum counterpart. The multi-baker map provides a convenient model for this study.

In order to set the stage for further work, we considered here the extreme quantum limit of the QMB where each unit cell contains just two quantum states, in either the position or momentum representation. Further work will now be devoted to the properties of the QMB for smaller values of  $h$ , including a study of the semi-classical regime where the Planck constant is very small, and the transition to the classical limit.

In order to explore a variety of versions of the QMB, we used the fact that the Weyl quantization procedure for maps on torus allows some freedom in the choice of phases for the quantum states. This freedom can be thought of as a freedom in the location of the quantum states in the position and momentum representations, or as the effects of Bohm-Aharonov current loops on the wave functions in each unit cell. For large  $h$  and for the regular QMB, we have been able to proceed with analytical calculations for the quasi-energies, and for the quantum states for different boundary conditions. These calculations showed ballistic transport of probability amplitudes within the chain, due to the Bloch wave structure of the eigenstates, as well as a slow decay of probability from an open, finite chain, due to the difficulty that long wavelength modes have in escaping through the exit channels. The random phase case exhibits localization of wave functions and the appropriate equations were shown to be close to the basic equations of the Anderson model of localization. All of these results show that the behavior of the QMB for  $N = 2$  is quite different from that of the classical multi-baker map, which exhibits normal, diffusive transport. For larger  $N$ , smaller  $h$ , we should see behavior that more closely approximates the classical behavior, at least on the logarithmic time scale.

There are quite a large number of directions for future studies of the QMB. For the case of  $h = 1/2$  we have studied only the regular and random phase cases. One can also consider models in which there is a well defined, systematic progression of phases from one cell to

the next, or where the phases in the cells are incommensurate (oscillating with irrational periods). The situation for larger  $N$  is such there are  $N$  quantum states in each cell, so that there will then be several transport channels in the QMB. It remains to be seen what the properties of these systems will be, both as functions of  $N$  as well as functions of the phases of the wave functions in the cells. As  $h$  approaches zero, one can study the semi-classical limit and the approach to classical, chaotic behavior of the QMB. Such a study should reveal for this simple system, at least, the role of decoherence for obtaining a proper chaotic limit. Clearly, we should obtain the diffusive behavior independently of the distribution of phases, that is both for the regular (ballistic) case, as well as for the random (localized) case. The QMB is simple enough to consider the classical limit for regular phase, random phase, and incommensurate phase model, among others. The investigation of these questions will be the subject of further papers in this series.

## Acknowledgments

This work has been partially supported through the NSF grant PHY-98-20824. Conversations with Robert Alicki, Jean Bellissard, Mark Fannes, Shmuel Fishman, Pierre Gaspard, Fritz Haake, Salman Habib, Ted Kirkpatrick, Shuichi Tasaki, Henk van Beijeren, Wojciech Żurek, Karol Życzkowski were of particular help. We thank the organizers of the 38th Winter School of Theoretical Physics “Dynamical Semigroups: Dissipation, Chaos, Quanta” in Łądek Zdrój, Poland, for providing us with an opportunity to present and discuss these results.

## APPENDIX A: EIGENVALUES OF THE OPEN QUANTUM MULTIBAKER LIE INSIDE THE UNIT CIRCLE

Due to the escape of probability density, the eigenvalues that determine the time dependence of the probability density in each cell move to the interior of the unit circle. A simple proof of this fact can be given as follows. Let  $\Psi(t = 0)$  be a normalized eigenstate of the open quantum multibaker. Since the multibaker dynamics requires that  $\tilde{\Psi}_b(n-1, t+1) = f_0 \Psi_l(n, t)$ ,  $\tilde{\Psi}_t(n+1, t+1) = f_0 \Psi_r(n, t)$ , for  $n = 1, \dots, L-2$ , it follows that

$$|\tilde{\Psi}_b(n-1, t+1)|^2 + |\tilde{\Psi}_t(n+1, t+1)|^2 = |\Psi_l(n, t)|^2 + |\Psi_r(n, t)|^2. \quad (\text{A1})$$

The probability of the system being in cell  $n$  is given by  $\varrho(n, t) := |\Psi_l(n, t)|^2 + |\Psi_r(n, t)|^2 = |\tilde{\Psi}_b(n, t)|^2 + |\tilde{\Psi}_t(n, t)|^2$ , where we have used the unitarity of the trans-

formation  $G_2^{-1}$ . In the boundary cells we have

$$\begin{cases} |\tilde{\Psi}_b(0, t+1)|^2 + |\tilde{\Psi}_l(L-1, t+1)|^2 = 0, \\ |\tilde{\Psi}_b(1, t+1)|^2 = |\Psi_l(0, t)|^2, \\ |\tilde{\Psi}_t(L-2, t+1)|^2 = |\Psi_r(L-1, t)|^2. \end{cases} \quad (\text{A2})$$

By adding up the equations (A1) for cells  $n = 1, 2, \dots, L-2$  and (A2) we obtain

$$\sum_{n=0}^{L-1} \varrho(n, t+1) = \sum_{n=0}^{L-1} \varrho(n, t) - (|\Psi_r(0, t)|^2 + |\Psi_l(L-1, t)|^2). \quad (\text{A3})$$

But  $\Psi$  is a normalized eigenstate at  $t = 0$ , therefore

$$\sum_{n=0}^{L-1} \varrho(n, 1) = |\lambda|^2 = 1 - (|\Psi_r(0, 0)|^2 + |\Psi_l(L-1, 0)|^2).$$

This implies  $1 - |\lambda|^2 = (|\Psi_r(0, 0)|^2 + |\Psi_l(L-1, 0)|^2) \geq 0$ . Thus  $0 \leq |\lambda|^2 \leq 1$ . Suppose now  $|\lambda|^2 = 1$ . Then  $\Psi_r(0, 0) = \Psi_l(L-1, 0) = 0$ . Thus, from Eq. (18) and (29)  $0 = \tilde{\Psi}_b(0, 0) = g_{01}\Psi_l(0, 0) \Rightarrow \Psi_l(0, 0) = \Psi_r(0, 0) = 0$ . It follows that also  $\Psi_t(0, 0) = 0$ . But  $\tilde{\Psi}_t(0, 0) = \lambda^{-1}\tilde{\Psi}_t(0, 1) = \lambda^{-1}f_0\Psi_r(1, 0)$ . Thus  $\Psi_r(1, 0) = 0$ . Also,  $\tilde{\Psi}_b(1, 1) = f_0\Psi_l(0, 0) = 0 = \lambda g_{01}\Psi_l(1, 0)$ . Therefore  $\Psi_l(1, 0) = \Psi_r(1, 0) = 0$ , and so on. Thus the assumption  $|\lambda|^2 = 1$  leads to the eigenstate being identically 0 which cannot be normalized. Therefore all of the eigenvalues lie inside the unit circle  $0 \leq |\lambda|^2 < 1$ . It is easy to identify the kernel of  $B_L$  since  $\lambda = 0$  implies  $|\Psi_r(0, 0)|^2 + |\Psi_l(L-1, 0)|^2 = 1$ . Thus the kernel is

spanned by vectors with 0 everywhere apart from  $\Psi_r(0)$  and  $\Psi_l(L-1)$ .

We are thus led to the conclusion that of the  $2L$  eigenstates exactly two span the kernel, and the eigenvalues corresponding to the remaining  $2L-2$  satisfy  $0 < |\lambda| < 1$ . Note that the above arguments are independent of the distribution of phases and thus apply also to the open random quantum multibaker. Generalization to arbitrary  $N$  is obvious.

## APPENDIX B: ANDERSON MODEL

Consider a one-dimensional Schrödinger equation on a lattice of lattice constant  $a$  [33]:

$$i\hbar\dot{\Psi}_n = -\frac{\hbar^2}{2ma^2}[\Psi_{n+1} + \Psi_{n-1} - 2\Psi_n] + V_n\Psi_n. \quad (\text{B1})$$

A time independent equation can be written as  $(\tilde{E} - \tilde{V}_n)\Psi_n = \Psi_{n+1} + \Psi_{n-1}$ , where  $\tilde{E} = 2 - 2ma^2E/\hbar^2$ ,  $\tilde{V}_n = 2ma^2V_n/\hbar^2$ . We can also write it using transfer matrices

$$\begin{bmatrix} \Psi_{n+1} \\ \Psi_n \end{bmatrix} = \begin{bmatrix} \tilde{E} - \tilde{V}_n & -1 \\ 1 & 0 \end{bmatrix} \begin{bmatrix} \Psi_n \\ \Psi_{n-1} \end{bmatrix}, \quad (\text{B2})$$

which has very similar form to the equation (92). A general discussion of one-dimensional disordered models can be found in [32, 34]

- 
- [1] M. C. Gutzwiller, *Chaos in classical and quantum mechanics* (Springer-Verlag, New York, 1990).
  - [2] H. J. Stöckmann, *Quantum Chaos. An Introduction* (Cambridge University Press, Cambridge, 1999).
  - [3] F. Haake, *Quantum Signatures of Chaos* (Springer Verlag, Berlin, New York, 2001), 2nd ed.
  - [4] P. Gaspard, *Chaos, scattering and statistical mechanics* (Cambridge University Press, Cambridge, 1998).
  - [5] S. Tasaki and P. Gaspard, J. Stat. Phys. **101**, 125 (2000).
  - [6] S. Tasaki and P. Gaspard, Theor. Chem. Acc. **102**, 385 (1999).
  - [7] T. Gilbert, J. R. Dorfman, and P. Gaspard, Phys. Rev. Lett. **85**(8), 1606 (2000).
  - [8] S. Tasaki and P. Gaspard, J. Stat. Phys. **81**(5/6), 935 (1995).
  - [9] P. Gaspard, J. Stat. Phys. **68**(5/6), 673 (1992).
  - [10] T. Gilbert and J. R. Dorfman, J. Stat. Phys. **96**(1/2), 225 (1999).
  - [11] J. Vollmer, T. Tel, and L. Matyas, J. Stat. Phys. **101**, 79 (2000).
  - [12] L. Matyas, T. Tel, and J. Vollmer, Phys. Rev. E **62**, 349 (2000).
  - [13] L. Rondoni, T. Tel, and J. Vollmer, Phys. Rev. E **61**, R4679 (2000).
  - [14] J. Vollmer, T. Tel, and W. Breyman, Phys. Rev. E **58**, 1672 (1998).
  - [15] W. Breyman, T. Tel, and J. Vollmer, Chaos **8**, 396 (1998).
  - [16] J. Vollmer, T. Tel, and W. Breyman, Phys. Rev. Lett. **79**, 2759 (1997).
  - [17] W. G. Breyman, T. Tel, and J. Vollmer, Phys. Rev. Lett. **77**, 2945 (1996).
  - [18] T. Tél and J. Vollmer, in *Hard Ball Systems and the Lorentz Gas*, edited by D. Szász (Springer Verlag, 2000), vol. 101 of *Encyclopaedia of Mathematical Sciences*, pp. 369–418.
  - [19] N. L. Balazs and A. Voros, Ann. Phys. **190**, 1 (1989).
  - [20] M. Saraceno, Ann. Phys. **199**, 37 (1990).
  - [21] D. K. Wójcik and J. R. Dorfman, *Transport in quantum multibakers* (2002), in preparation.
  - [22] D. K. Wójcik and J. R. Dorfman, *Quantum multibaker maps II: Semi-classical Limit* (2002), in preparation.
  - [23] J. H. Hannay and M. V. Berry, Physica D **1**, 267 (1980).
  - [24] S. DeBievre, M. D. Esposti, and R. Giachetti, Commun. Math. Phys. **176**, 73 (1996).
  - [25] Y. Aharonov, L. Davidovich, and N. Zagury, Phys Rev A **48**(2), 1687 (1993).
  - [26] S. Godoy and S. Fujita, J. Chem. Phys. **97**, 5148 (1992).
  - [27] S. Godoy and L. S. Garcia-Colin, Phys. Rev. E **53**, 5779 (1996).



- [28] F. Barra and P. Gaspard, J. Phys. A **32**, 3357 (1999).
- [29] P. Gaspard and G. Nicolis, Phys. Rev. Lett. **65**(14), 1693 (1990).
- [30] J. R. Dorfman, *An introduction to chaos in nonequilibrium statistical mechanics* (Cambridge University Press, Cambridge, 1999).
- [31] C. M. Bender and S. A. Orszag, *Advanced mathematical methods for scientists and engineers* (Mc-Graw Hill, New York, 1978), chap. 7, p. 319.
- [32] A. Crisanti, G. Paladin, and A. Vulpiani, *Products of random matrices in statistical physics*, vol. 104 of *Springer series in solid-state sciences* (Springer, Berlin, New York, 1993).
- [33] P. W. Anderson, Phys. Rev. **109**, 1492 (1958).
- [34] K. Ishii, Suppl. Progr. Theor. Phys. Kyoto **53**, 77 (1973).
- [35] P. Gaspard has suggested that the phases used here may be thought of as resulting from vector potentials produced by thin solenoids, which modify the phases of the wave-functions through Bohm-Aharonov loops.
- [36] Remaining values  $k = L + 1, \dots, 2L - 1$  lead to  $u \rightarrow 1/u$  which gives the same  $v$  and thus they are discarded.